Editors' Suggestion

Laser Cooling of a Nanomechanical Oscillator to Its Zero-Point Energy

Liu Qiu,[1] Itay Shomroni,[1] Paul Seidler,[2,*] and Tobias J. Kippenberg[1,†]
[1]Institute of Physics, Swiss Federal Institute of Technology Lausanne (EPFL), Station 3, CH-1015 Lausanne, Switzerland
[2]IBM Research–Zurich, Säumerstrasse 4, CH-8803 Rüschlikon, Switzerland

(Received 2 April 2019; revised manuscript received 18 December 2019; accepted 23 March 2020; published 29 April 2020)

Optomechanical systems in the well-resolved-sideband regime are ideal for studying a myriad of quantum phenomena with mechanical systems, including backaction-evading measurements, mechanical squeezing, and nonclassical states generation. For these experiments, the mechanical oscillator should be prepared in its ground state, i.e., exhibit negligible residual excess motion compared to its zero-point motion. This can be achieved using the radiation pressure of laser light in the cavity by selectively driving the lower motional sideband, leading to sideband cooling. To date, the preparation of sideband-resolved optical systems to their zero-point energy has eluded laser cooling because of strong optical absorption heating. The alternative method of passive cooling suffers from the same problem, as the requisite milliKelvin environment is incompatible with the strong optical driving needed by many quantum protocols. Here, we employ a highly sideband-resolved silicon optomechanical crystal in a ^{3}He buffer-gas environment at $\sim$2 K to demonstrate laser sideband cooling to a mean thermal phonon occupancy of $0.09^{+0.02}_{-0.01}$ quantum (self-calibrated using motional sideband asymmetry), which is -7.4 dB of the oscillator's zero-point energy and corresponds to 92% ground state probability. Achieving such low occupancy by laser cooling opens the door to a wide range of quantum-optomechanical experiments in the optical domain.

DOI: 10.1103/PhysRevLett.124.173601

Laser cooling techniques developed several decades ago [1–4] have revolutionized many areas of science and technology, with systems ranging from atoms, ions, and molecules [5–11] to solid-state structures and macroscopic mechanical objects [12–15]. Among these systems, mechanical oscillators play a unique role given their macroscopic nature and their ability to couple to diverse physical quantities [15]. Laser cooling of mechanical systems can be achieved via coupling of mechanical and electromagnetic degrees of freedom and has been demonstrated with a wide range of structures [12,16–25]. It has enabled the observation of radiation pressure shot noise [26], motional sideband asymmetry [16,27–30], ponderomotive squeezing of light [29,31,32], quantum coherent coupling [21], and mechanical quantum feedback [22,25].

Many optomechanical protocols for quantum phenomena, such as mechanical squeezing [33–36], entanglement [37], generation of nonclassical states [38–41], and backaction evading (BAE) measurements below the standard quantum limit (SQL) [42–44], require ground state preparation of a well-sideband-resolved system, where Stokes and anti-Stokes motional transitions can be driven selectively. In this case, driving of anti-Stokes transitions can be efficiently applied to damp the motion and sideband cool the system. The cooling limit is set by laser noise (classical [45–48] or quantum [16,17,23]) or by technical limitations such as absorption heating, and determines the final residual mean number of thermal quanta $\bar{n}_f$. Importantly, for the case of mechanical squeezing or BAE measurements, $\bar{n}_f \ll 0.5$ is required—i.e., the mechanical oscillator is required to exhibit negligible residual excess energy compared to the zero-point energy—with the amount that $\bar{n}_f$ is below 0.5 setting the achievable amount of mechanical squeezing or the extent to which the SQL on resonance can be surpassed. Such deep ground-state preparation has been demonstrated in microwave optomechanical systems [20]. In the optical domain, cooling to $\bar{n}_f < 0.5$ has so far only been achieved in systems that are not sideband resolved, i.e., cooling to the bad-cavity limit [23] or using feedback cooling [25].

One type of optomechanical system that can operate deeply in the resolved sideband regime is a silicon optomechanical crystal (OMC) [49,50]. OMCs that couple an optical mode at telecommunication wavelengths and a colocalized mechanical mode at GHz frequencies exhibit several exceptional features, including large vacuum coupling rates $\mathcal{O}(1\ \mathrm{MHz})$ [50] as well as ultralong phonon lifetime [51]. They have been employed in a wide range of experiments, such as continuous quantum measurements [19,30,44], and probabilistic preparation of quantum states [38–40]. The compatibility of these systems with nanofabrication technology and their scalability have motivated studies of optomechanical topological phenomena [52,53], frequency conversion [54], and coupling to superconducting qubits [55,56]. Yet despite these promising features,

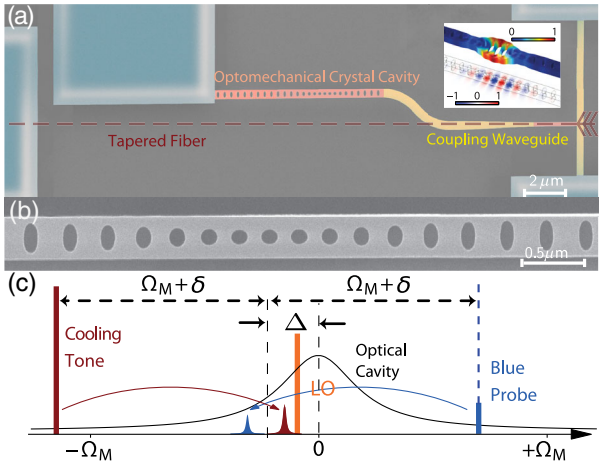

FIG. 1. Optomechanical crystal and experimental scheme. (a) False-color SEM image of the silicon OMC with a waveguide for input coupling of light. The path of the tapered fiber is indicated by the red dashed line. The inset shows the simulated mechanical breathing mode and optical mode. (b) SEM image of the central portion of the silicon OMC. (c) Measurement scheme using a cooling tone for sideband cooling and a blue probe for motional sideband asymmetry measurement. The local oscillator (LO) is used for detection and is not sent to the cavity.

deep ground-state preparation, $\bar{n}_f \ll 0.5$, has only been possible via passive cooling to milliKelvin temperatures in dilution refrigerators [57,58]. Significant heating due to optical absorption—a consequence of the extremely small optical mode volume and inefficient thermalization [59]—has limited experiments to the use of weak laser pulses [38–40,51] and precluded continuous measurements [30,44,57].

In this work, we demonstrate laser cooling of a strongly sideband-resolved silicon OMC to the zero-point energy, with residual mean phonon occupancy of $0.09^{+0.02}_{-0.01}$ (i.e., −7.4 dB of the zero-point energy). The measurement is self-calibrated using motional sideband asymmetry [16,28,30,60,61]. Our experimental system, shown in Figs. 1(a) and 1(b), consists of a quasi-one-dimensional silicon optomechanical crystal [30,44,50]. The OMC is mounted in a ^{3}He cryostat (Oxford Instruments HelioxTL) operated at ∼2.0 K and a buffer-gas pressure of ∼40 mbar, which ensures efficient thermalization of the device [30,44]. A tapered optical fiber is used to couple light evanescently into the coupling waveguide (40% efficiency in this work). We monitor the laser light reflected from the single-sided optical cavity. The optical resonance is at 1540 nm with a total linewidth of $\kappa/2\pi \simeq 255$ MHz, of which the external coupling rate is $\kappa_{ex}/2\pi \simeq 71$ MHz. The optical mode is coupled to a localized mechanical mode with frequency $\Omega_m/2\pi \simeq 5.17$ GHz and an intrinsic damping rate of $\Gamma_{int}/2\pi \simeq 65$ kHz. The measured vacuum optomechanical coupling rate is $g_0/2\pi \simeq 1080$ kHz. The buffer gas causes additional damping, increasing the mechanical linewidth to $\Gamma_m = \Gamma_{int} + \Gamma_{gas} \simeq 2\pi \times 115$ kHz [62].

Motional sideband asymmetry, a signature of the quantum nature of the optomechanical interaction, was recently observed in various optomechanical systems [27–29] and used to perform self-calibrated thermometry of the mechanical oscillator close to its ground state [30,60,61]. In our experiments, we adopt a two-tone pumping scheme [Fig. 1(c)], where a strong cooling tone near the lower motional sideband is applied for sideband cooling, while an additional weaker "blue probe" is applied near the upper motional sideband. By measuring the resonantly enhanced anti-Stokes and Stokes scattered sidebands, proportional to $\bar{n}_f$ and $\bar{n}_f + 1$, the mean phonon occupancy of the oscillator $\bar{n}_f$ can be determined. The frequencies of the two tones are separated by $2(\Omega_m + \delta)$, and their mean is detuned from the optical resonance frequency by Δ [Fig. 1(c)]. The radiation pressure from the two tones modifies the mechanical susceptibility. The effective mechanical damping rate becomes $\Gamma_{eff} = \Gamma_m + \Gamma_{opt}$, with the total optomechanical damping rate (in the resolved-sideband regime) $\Gamma_{opt} = -\Gamma_b + \Gamma_c$, where

$$\Gamma_{b(c)} = \bar{n}_{b(c)} g_0^2 \left(\frac{\kappa}{\kappa^2/4 + (\Delta \pm \delta)^2} \right), \tag{1}$$

and $\bar{n}_b$ and $\bar{n}_c$ are the mean intracavity photon numbers of the blue probe and cooling tone, respectively. In the weak coupling regime, $\Gamma_{opt} \ll \kappa$, the effective mechanical frequency is $\Omega_{eff} = \Omega_m + \delta\Omega_m$, with

$$\delta\Omega_m = g_0^2 \left(\bar{n}_b \frac{\Delta + \delta}{\kappa^2/4 + (\Delta + \delta)^2} + \bar{n}_c \frac{\Delta - \delta}{\kappa^2/4 + (\Delta - \delta)^2} \right). \tag{2}$$

The mean final phonon occupancy is given by

$$\bar{n}_f = \frac{\Gamma_m \bar{n}_{th} + \Gamma_b}{\Gamma_{eff}}, \tag{3}$$

where $\bar{n}_{th}$ is the mean phonon occupancy due to the thermal environment. The second term in the numerator of Eq. (3) corresponds to quantum backaction (QBA) heating due to resonant Stokes transitions from the blue probe [Fig. 1(c)], which can not be neglected since it can be comparable to the heating rate by the thermal bath at high probe powers and limits the mean final occupancy to $\bar{n}_f = \Gamma_b/\Gamma_{eff}$ [62]. This is in contrast to the quantum backaction limit due to the cooling tone, which is completely negligible in the well-resolved sideband regime (here $\Omega_m/\kappa \simeq 20$) [16,17,23,24]. Thus we perform both two-tone measurements for ancillary quantum thermometry and single-tone measurements to achieve the lowest possible occupancy.

In each measurement, we first determine the detuning of the cooling tone from the cavity, $\Delta_c = \Delta - \Omega_m - \delta$ by performing a coherent cavity response measurement [44,66]. We then obtain the thermomechanical noise spectrum by measuring the cavity output field using quantum-limited balanced heterodyne detection (BHD) with a strong phase-locked local

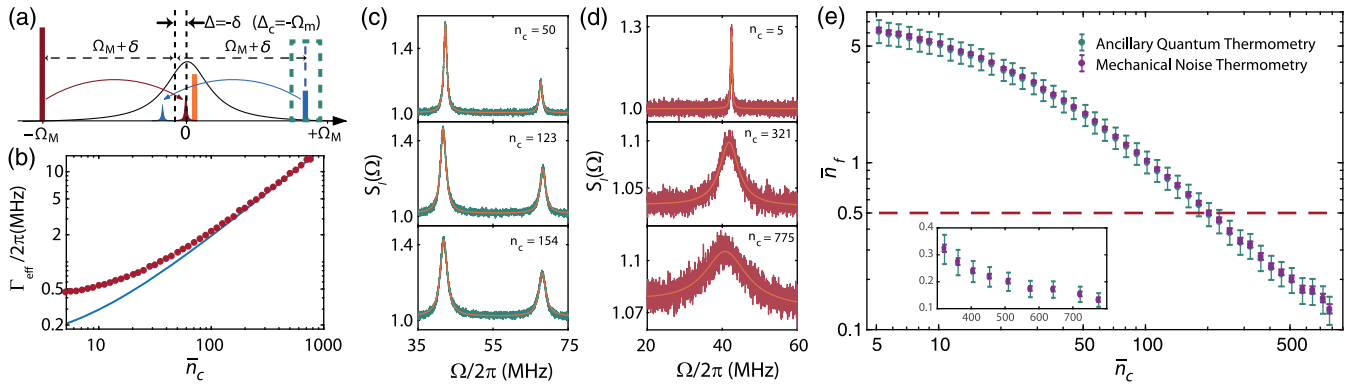

FIG. 2. Power dependence of sideband cooling. (a) Pumping scheme for the power sweep with a cooling tone at a fixed detuning of $-\Omega_m$ relative to the cavity resonance and an additional blue probe for sideband asymmetry calibration, as indicated in the dashed green box. The frequency separation between the cooling tone and blue probe is fixed at $2(\Omega_m + \delta)$. (b) Measured effective mechanical linewidth $\Gamma_{\rm eff}$ from the noise power spectral density vs cooling tone intracavity photon number $\bar{n}_c$ (red full circles) in single-tone measurements with a theoretical plot with experimental values (blue curve). (c) and (d) Single-sided noise spectra from balanced heterodyne detection normalized to the shot noise floor from two-tone and single-tone measurements, respectively, with corresponding fit curves, for various intracavity photon numbers. (e) Final phonon occupancy vs intracavity photon number of the cooling tone in single tone measurements. Purple full circles are anchored to the cryostat thermometer temperature at the lowest values of $\bar{n}_c$. Green full circles utilize the averaged calibration coefficient obtained from the ancillary two-tone sideband-asymmetry measurements, where the error bars are given by both the errors in the Lorentzian fit and in the calibration coefficient. The inset shows an expanded view at the highest cooling powers. The horizontal red dashed line corresponds to $\bar{n}_f = 1/2$.

oscillator [(LO); ~8 mW]. The frequency difference between the LO and the mean frequency of the two pumping tones is $\Delta_{\rm LO}$, where $0 < -\delta < \Delta_{\rm LO}$. The measured heterodyne noise spectrum, normalized to the shot noise floor, is given by

$$S_I(\Omega) = 1 + \eta\Gamma_{\rm eff}\left[\frac{(\bar{n}_f+1)\Gamma_b}{\Gamma_{\rm eff}^2/4 + (\Omega+\delta-\Delta_{\rm LO})^2} + \frac{\bar{n}_f\Gamma_c}{\Gamma_{\rm eff}^2/4 + (\Omega-\delta-\Delta_{\rm LO})^2}\right], \quad (4)$$

where η is the overall detection efficiency. The second and third terms in Eq. (4) correspond to the scattered Stokes and anti-Stokes sidebands, which we use for self-calibrated quantum noise thermometry of the oscillator.

Our scheme differs from previous experiments that utilize equal red and blue probes alongside a cooling tone [28,30]. By using only two tones, we avoid coupling between scattered sidebands due to Floquet dynamics that may corrupt the sideband asymmetry [30]. We keep the ratio between the input powers of the cooling tone and the blue probe around 6, to achieve both sufficient cooling and a measurable anti-Stokes signal ($\propto \bar{n}_f$). From a series of two-tone measurements, we obtain a mean calibration coefficient between the normalized thermomechanical sideband area A_c/Γ_c and the phonon occupancy $\bar{n}_f$ using Eq. (4), where A_c is the area of the sideband from the cooling tone [62]. The calibration coefficient serves as an ancillary quantum thermometer for the mechanical mode, independent of the resistive thermometer mounted in the cryostat. For ground state cooling, we turn off the blue probe and perform single-tone sideband cooling measurements, keeping the same experimental conditions and calibration. From the measured thermomechanical noise spectrum, we can thus obtain the final occupancy using two independent calibrations, i.e., the ancillary quantum thermometry and the mechanical noise thermometry, where for the latter the mechanical mode temperature is referenced to the cryostat thermometer [62].

In the first set of measurements, we vary the power of the pump tones while keeping $\Delta_c = -\Omega_m$ fixed for optimal sideband cooling. A blue probe, as indicated in the dashed green box in Fig. 2(a), is utilized only for ancillary sideband asymmetry measurements. Figure 2(b) shows the effective mechanical linewidth $\Gamma_{\rm eff}$ as a function of the cooling-tone intracavity photon number $\bar{n}_c$, obtained from the noise spectra in the single-tone experiments (red full circles) with a theoretical plot (blue curve) assuming a mechanical linewidth $\Gamma_m/2\pi = 115$ kHz and vacuum coupling rate $g_0/2\pi = 1080$ kHz. As shown in Fig. 2(b), $\Gamma_{\rm eff}$ deviates from the theoretical value for low intracavity photon numbers. We attribute this to condensed ^{3}He on the surface of the OMC, which degrades the mechanical linewidth at low powers but may improve the thermalization [62]. Figures 2(c) and 2(d) show a series of noise spectra normalized to the shot noise from the two-tone and single-tone measurements, respectively, at various values of $\bar{n}_c$ along with Lorentzian fits [62]. The left and right thermomechanical sidebands shown in Fig. 2(c) are from the cooling tone and the blue probe, respectively. We choose a series of pumping powers that ensures both sufficient laser cooling and measurable, nonoverlapping Stokes and anti-Stokes sidebands [28]. As the power increases, the ratio of the areas of the red and blue

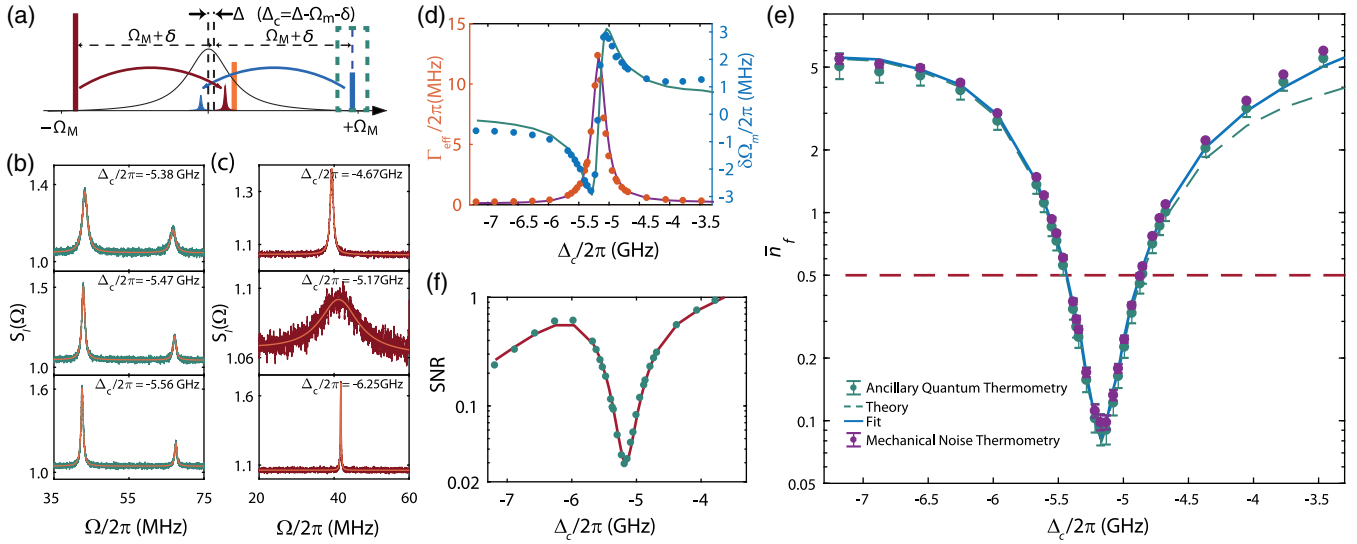

FIG. 3. Detuning dependence of the sideband cooling. (a) Pumping scheme for the detuning sweep where the detuning Δ_c of the cooling tone relative to the cavity resonance is varied. An additional blue probe is used for ancillary sideband asymmetry calibration, as indicated in the dashed green box. Frequency separation between the cooling tone and blue probe is fixed at $2(\Omega_m + \delta)$. (b) and (c) Single-sided noise spectra from the balanced heterodyne detection normalized to the shot noise floor from two-tone and single-tone measurements, respectively, with corresponding fit curves, for various detunings. (d) The fitted mechanical linewidth (red full circles, left axis) and optical spring effect (blue full circles, right axis), with corresponding theoretical plots based on experimental optomechanical parameters. (e) Final phonon occupancy vs Δ_c in single-tone measurements. Green full circles show calibration using the ancillary two-tone quantum thermometry. Dashed green curve shows a theoretical plot calculated from experimental optomechanical parameters assuming ideal thermalization. Blue curve shows a fitting curve incorporating excess optical heating. Error bars are given by the errors in the Lorentzian fits and in the calibration coefficient in two-tone sideband asymmetry. Purple full circles are anchored with cryostat thermometer at $\Delta_c/2\pi \simeq -7.18$ GHz. (f) Signal-to-noise ratio (SNR) vs Δ_c, with the fitting curve to a theoretical model which includes optical heating, with excess heating rate and overall detection efficiency as free fitting parameters.

sidebands, given by $\bar{n}_f\Gamma_c/(\bar{n}_f+1)\Gamma_b$ [cf. Eq. (4)], decreases as the mechanical oscillator approaches the ground state ($\bar{n}_f \to 0$), as shown in Fig. 2(c). We thus obtain an averaged calibration coefficient between the normalized thermomechanical sideband area and the final occupancy from a series of ancillary quantum thermometry measurements [62]. At high pumping powers, we observe an increase in the noise floor, as evident in the middle and bottom panels in Fig. 2(d). This originates from beating of the high signal power with excess noise of the LO around 5.17 GHz [62]. Figure 2(e) shows the inferred mean phonon occupancy $\bar{n}_f$ vs $\bar{n}_c$ from the single-tone measurements, calibrated using two independent methods. The green circles show the phonon occupancy calibrated using the ancillary sideband asymmetry measurements. The purple full circles show the calibration using the cryostat thermometer by anchoring the lowest value of $\bar{n}_c \sim 5$ at 2.0 K. This requires knowledge of Γ_m, which is estimated by subtracting the calculated value of $\Gamma_{\rm opt}$ at this power from the measured $\Gamma_{\rm eff}$, to yield $\Gamma_m/2\pi \simeq 360$ kHz. We note that Γ_m is unnecessary using ancillary quantum thermometry, making it an ideal independent quantum thermometer, as opposed to conventional mechanical noise thermometry [62]. The two methods show excellent agreement. The minimum phonon occupancy achieved in this power-sweep experiment is $0.13^{+0.02}_{-0.02}$ (88% ground-state occupancy) and is reached at a cooling-tone intracavity photon number $\bar{n}_c \approx 776$.

In a second set of measurements, we keep the power constant but vary the detuning Δ_c of the cooling tone with respect to the cavity resonance, keeping the frequency separation of the blue probe in the ancillary measurement and that of the LO fixed at $2(\Omega_m+\delta)$ and $\Delta_{\rm LO}$, respectively [Fig. 3(a)]. Figures 3(b) and 3(c) each show a series of measured noise spectra normalized to the shot noise floor at various values of Δ_c, together with Lorentzian fits, from the two-tone and single-tone measurements. In the ancillary two-tone measurements, the input powers of the cooling tone and blue probe are ~350 μW and ~60 μW, respectively, with a series of values of Δ_c to ensure sufficient laser cooling and measurable, nonoverlapping Stokes and anti-Stokes sidebands. To infer $\bar{n}_f$ via sideband thermometry, the detuning-dependent intracavity photon number and optical susceptibility for the two scattered sidebands must be taken into consideration. We obtain a mean calibration coefficient between the normalized thermomechanical sideband area and the final occupancy from the sideband asymmetry measurements. For single-tone measurements, the cooling tone input power is ~500 μW. Figure 3(d) shows the effective mechanical linewidth (red circles) and

the optical spring effect (blue circles) obtained from a Lorentzian fit to the noise spectrum, with excellent agreement with the respective theoretical curves. We note that, due to the presence of high input power throughout the measurement, the mechanical linewidth degradation observed at low powers in the previous measurement [Fig. 2(b)] is absent. Figure 3(e) shows $\bar{n}_f$ vs Δ_c, where $\bar{n}_f$ is calibrated from the thermomechanical sideband area from the single-tone sideband cooling measurements. Green circles are determined using the mean calibration factor obtained from sideband asymmetry measurements. The theoretical dependence calculated from experimental parameters [Eq. (3)] is shown as a green dashed curve for comparison. The theory curve is in excellent agreement with the data except in the region where the cooling tone approaches the cavity resonance, indicating residual optical heating [30,57]. We fit the phonon occupancy with a model incorporating heating [blue curve in Fig. 3(e)] that is both linear and quadratic in the number of intracavity photons [62]. The fit indicates that the excess optical heating in our measurements has primarily a quadratic dependence, resulting in an increase in $\bar{n}_{\mathrm{th}}$ of $\sim 1.2 \times 10^{-6} \bar{n}_c^2$; the linear coefficient is negligible. This is different from previous experiments with large optical decay rate, where linear absorption heating dominates [30]. The quadratic dependence is suggestive of two-photon absorption [67,68]. We note that in any case such optical heating cannot come from excess laser noise [45–48], for which the heating rate peaks at $\Delta_c = -\Omega_m$. For the noise thermometry, we anchor the calibration to 2.0 K, at a farthest detuning of $\Delta_c/2\pi \approx -7.18$ GHz. The resulting data are shown as purple full circles in Fig. 3(e). For $\Delta_c/2\pi = -7.18$ GHz with $\bar{n}_c = 330$, the estimated increase in $\bar{n}_{\mathrm{th}}$ due to quadratic heating is ~ 0.135, which is negligible compared to the bare thermal bath occupation of 8.2 phonons. This indicates that the mechanical oscillator is well thermalized despite the high pumping power. The minimum phonon occupancy, occurring close to the red mechanical sideband ($\Delta_c/2\pi \simeq -5.17$ GHz), is $\bar{n}_f = 0.09^{+0.02}_{-0.01}$ (92% ground state occupation), which is -7.4 dB of the zero-point energy. In Fig. 3(f), the signal-to-noise ratio vs Δ_c for the thermomechanical noise spectrum is shown with a fit that includes the quadratic heating [62], which yields an overall detection efficiency $\eta \simeq 6.4\%$.

In conclusion, we have demonstrated high-fidelity sideband cooling to the zero-point energy of a localized GHz mechanical mode of a silicon OMC. The residual mean phonon occupancy is $0.09^{+0.02}_{-0.01}$ (92% ground state occupation). The system possesses a unique blend of advantageous properties, combining high mechanical frequency, large sideband resolution, negligible optical-absorption heating, and the ability to be prepared in the ground state in the presence of strong probing. These characteristics enable a large number of quantum optomechanical experiments in the optical domain, including two-tone backaction-evading measurements reaching sub-SQL sensitivity [43,44,69], squeezed mechanical states [33–36,70], low-added-noise optomechanical transducers [54,71,72], as well as quantum-coherent operations [37,73,74].

All data and analysis files are available via [75].

This work is supported by the European Unions Horizon 2020 research and innovation programme under Grant No. 732894 (FET Proactive HOT). T. J. K. acknowledges funding from European Research Council (ERC) under the European Union Horizon 2020 research and innovation programme, Grant Agreement No. 835329 (ExCOM-cCEO). Samples were fabricated in the Binnig and Rohrer Nanotechnology Center at IBM Research–Zurich and at the Center of MicroNanoTechnology (CMi) at EPFL.

L. Q. and I. S. contributed equally to this work.

*pfs@zurich.ibm.com
†tobias.kippenberg@epfl.ch

[1] S. Chu, Rev. Mod. Phys. **70**, 685 (1998).
[2] C. N. Cohen-Tannoudji, Rev. Mod. Phys. **70**, 707 (1998).
[3] C. E. Wieman, D. E. Pritchard, and D. J. Wineland, Rev. Mod. Phys. **71**, S253 (1999).
[4] T. J. Kippenberg and K. J. Vahala, Science **321**, 1172 (2008).
[5] A. Ashkin, Phys. Rev. Lett. **40**, 729 (1978).
[6] D. J. Wineland and W. M. Itano, Phys. Rev. A **20**, 1521 (1979).
[7] E. S. Shuman, J. F. Barry, and D. Demille, Nature (London) **467**, 820 (2010).
[8] L. Anderegg, B. L. Augenbraun, Y. Bao, S. Burchesky, L. W. Cheuk, W. Ketterle, and J. M. Doyle, Nat. Phys. **14**, 890 (2018).
[9] C. Ospelkaus, U. Warring, Y. Colombe, K. R. Brown, J. M. Amini, D. Leibfried, and D. J. Wineland, Nature (London) **476**, 181 (2011).
[10] C. Monroe and J. Kim, Science **339**, 1164 (2013).
[11] R. Blatt and C. F. Roos, Nat. Phys. **8**, 277 (2012).
[12] A. Schliesser, P. Del'Haye, N. Nooshi, K. J. Vahala, and T. J. Kippenberg, Phys. Rev. Lett. **97**, 243905 (2006).
[13] O. Arcizet, P.-F. Cohadon, T. Briant, M. Pinard, and A. Heidmann, Nature (London) **444**, 71 (2006).
[14] LIGO Scientific Collaboration, New J. Phys. **11**, 073032 (2009).
[15] M. Aspelmeyer, T. J. Kippenberg, and F. Marquardt, Rev. Mod. Phys. **86**, 1391 (2014).
[16] I. Wilson-Rae, N. Nooshi, W. Zwerger, and T. J. Kippenberg, Phys. Rev. Lett. **99**, 093901 (2007).
[17] F. Marquardt, J. P. Chen, A. A. Clerk, and S. M. Girvin, Phys. Rev. Lett. **99**, 093902 (2007).
[18] A. Schliesser, R. Rivière, G. Anetsberger, O. Arcizet, and T. J. Kippenberg, Nat. Phys. **4**, 415 (2008).
[19] J. Chan, T. P. Alegre, A. H. Safavi-Naeini, J. T. Hill, A. Krause, S. Gröblacher, M. Aspelmeyer, and O. Painter, Nature (London) **478**, 89 (2011).

[20] J. D. Teufel, T. Donner, D. Li, J. W. Harlow, M. S. Allman, K. Cicak, A. J. Sirois, J. D. Whittaker, K. W. Lehnert, and R. W. Simmonds, Nature (London) **475**, 359 (2011).

[21] E. Verhagen, S. Deléglise, S. Weis, A. Schliesser, and T. J. Kippenberg, Nature (London) **482**, 63 (2012).

[22] D. J. Wilson, V. Sudhir, N. Piro, R. Schilling, A. Ghadimi, and T. J. Kippenberg, Nature (London) **524**, 325 (2015).

[23] R. W. Peterson, T. P. Purdy, N. S. Kampel, R. W. Andrews, P. L. Yu, K. W. Lehnert, and C. A. Regal, Phys. Rev. Lett. **116**, 063601 (2016).

[24] J. B. Clark, F. Lecocq, R. W. Simmonds, J. Aumentado, and J. D. Teufel, Nature (London) **541**, 191 (2017).

[25] M. Rossi, D. Mason, J. Chen, Y. Tsaturyan, and A. Schliesser, Nature (London) **563**, 53 (2018).

[26] T. P. Purdy, R. W. Peterson, and C. A. Regal, Science **339**, 801 (2013).

[27] A. H. Safavi-Naeini, J. Chan, J. T. Hill, Thiago P. Mayer Alegre, A. Krause, and O. Painter, Phys. Rev. Lett. **108**, 033602 (2012).

[28] A. J. Weinstein, C. U. Lei, E. E. Wollman, J. Suh, A. Metelmann, A. A. Clerk, and K. C. Schwab, Phys. Rev. X **4**, 041003 (2014).

[29] V. Sudhir, D. J. Wilson, R. Schilling, H. Schütz, S. A. Fedorov, A. H. Ghadimi, A. Nunnenkamp, and T. J. Kippenberg, Phys. Rev. X **7**, 011001 (2017).

[30] L. Qiu, I. Shomroni, M. A. Ioannou, N. Piro, D. Malz, A. Nunnenkamp, and T. J. Kippenberg, Phys. Rev. A **100**, 053852 (2019).

[31] A. H. Safavi-Naeini, S. Gröblacher, J. T. Hill, J. Chan, M. Aspelmeyer, and O. Painter, Nature (London) **500**, 185 (2013).

[32] T. P. Purdy, P.-L. Yu, R. W. Peterson, N. S. Kampel, and C. A. Regal, Phys. Rev. X **3**, 031012 (2013).

[33] A. Kronwald, F. Marquardt, and A. A. Clerk, Phys. Rev. A **88**, 063833 (2013).

[34] F. Lecocq, J. B. Clark, R. W. Simmonds, J. Aumentado, and J. D. Teufel, Phys. Rev. X **5**, 041037 (2015).

[35] E. E. Wollman, C. U. Lei, A. J. Weinstein, J. Suh, A. Kronwald, F. Marquardt, A. A. Clerk, and K. C. Schwab, Science **349**, 952 (2015).

[36] J. M. Pirkkalainen, E. Damskägg, M. Brandt, F. Massel, and M. A. Sillanpää, Phys. Rev. Lett. **115**, 243601 (2015).

[37] C. F. Ockeloen-Korppi, E. Damskägg, J. M. Pirkkalainen, M. Asjad, A. A. Clerk, F. Massel, M. J. Woolley, and M. A. Sillanpää, Nature (London) **556**, 478 (2018).

[38] R. Riedinger, S. Hong, R. A. Norte, J. A. Slater, J. Shang, A. G. Krause, V. Anant, M. Aspelmeyer, and S. Gröblacher, Nature (London) **530**, 313 (2016).

[39] S. Hong, R. Riedinger, I. Marinković, A. Wallucks, S. G. Hofer, R. A. Norte, M. Aspelmeyer, and S. Gröblacher, Science **358**, 203 (2017).

[40] I. Marinković, A. Wallucks, R. Riedinger, S. Hong, M. Aspelmeyer, and S. Gröblacher, Phys. Rev. Lett. **121**, 220404 (2018).

[41] I. Shomroni, L. Qiu, and T. J. Kippenberg, Phys. Rev. A **101**, 033812 (2020).

[42] A. A. Clerk, F. Marquardt, and K. Jacobs, New J. Phys. **10**, 095010 (2008).

[43] J. Suh, A. J. Weinstein, C. U. Lei, E. E. Wollman, S. K. Steinke, P. Meystre, A. A. Clerk, and K. C. Schwab, Science **344**, 1262 (2014).

[44] I. Shomroni, L. Qiu, D. Malz, A. Nunnenkamp, and T. J. Kippenberg, Nat. Commun. **10**, 2086 (2019).

[45] P. Rabl, C. Genes, K. Hammerer, and M. Aspelmeyer, Phys. Rev. A **80**, 063819 (2009).

[46] A. M. Jayich, J. C. Sankey, K. Børkje, D. Lee, C. Yang, M. Underwood, L. Childress, A. Petrenko, S. M. Girvin, and J. G. E. Harris, New J. Phys. **14**, 115018 (2012).

[47] A. H. Safavi-Naeini, J. Chan, J. T. Hill, S. Gröblacher, H. Miao, Y. Chen, M. Aspelmeyer, and O. Painter, New J. Phys. **15**, 035007 (2013).

[48] T. J. Kippenberg, A. Schliesser, and M. L. Gorodetsky, New J. Phys. **15**, 015019 (2013).

[49] M. Eichenfield, J. Chan, R. M. Camacho, K. J. Vahala, and O. Painter, Nature (London) **462**, 78 (2009).

[50] J. Chan, A. H. Safavi-Naeini, J. T. Hill, S. Meenehan, and O. Painter, Appl. Phys. Lett. **101**, 081115 (2012).

[51] G. S. MacCabe, H. Ren, J. Luo, J. D. Cohen, H. Zhou, A. Sipahigil, M. Mirhosseini, and O. Painter, arXiv:1901.04129.

[52] M. Schmidt, S. Kessler, V. Peano, O. Painter, and F. Marquardt, Optica **2**, 635 (2015).

[53] C. Brendel, V. Peano, O. J. Painter, and F. Marquardt, Proc. Natl. Acad. Sci. U.S. A. **114**, E3390 (2017).

[54] K. Fang, M. H. Matheny, X. Luan, and O. Painter, Nat. Photonics **10**, 489 (2016).

[55] A. J. Keller, P. B. Dieterle, M. Fang, B. Berger, J. M. Fink, and O. Painter, Appl. Phys. Lett. **111**, 042603 (2017).

[56] P. Arrangoiz-Arriola, E. A. Wollack, M. Pechal, J. D. Witmer, J. T. Hill, and A. H. Safavi-Naeini, Phys. Rev. X **8**, 031007 (2018).

[57] S. M. Meenehan, J. D. Cohen, S. Gröblacher, J. T. Hill, A. H. Safavi-Naeini, M. Aspelmeyer, and O. Painter, Phys. Rev. A **90**, 011803(R) (2014).

[58] S. M. Meenehan, J. D. Cohen, G. S. MacCabe, F. Marsili, M. D. Shaw, and O. Painter, Phys. Rev. X **5**, 041002 (2015).

[59] M. G. Holland, Phys. Rev. **132**, 2461 (1963).

[60] T. P. Purdy, P.-L. Yu, N. S. Kampel, R. W. Peterson, K. Cicak, R. W. Simmonds, and C. A. Regal, Phys. Rev. A **92**, 031802(R) (2015).

[61] M. Underwood, D. Mason, D. Lee, H. Xu, L. Jiang, A. B. Shkarin, K. Børkje, S. M. Girvin, and J. G. E. Harris, Phys. Rev. A **92**, 061801(R) (2015).

[62] See Supplemental Material at http://link.aps.org/supplemental/10.1103/PhysRevLett.124.173601 for the theory, experimental details, and data analysis, which includes Refs. [63–65].

[63] K. Børkje, Phys. Rev. A **94**, 043816 (2016).

[64] A. J. Weinstein, Quantum electromechanics with two tone drive, Ph.D. Thesis, California Institute of Technology, 2016.

[65] S. Weis, R. Rivière, S. Deléglise, E. Gavartin, O. Arcizet, A. Schliesser, and T. J. Kippenberg, Science **330**, 1520 (2010).

[66] A. H. Safavi-Naeini, T. P. Alegre, J. Chan, M. Eichenfield, M. Winger, Q. Lin, J. T. Hill, D. E. Chang, and O. Painter, Nature (London) **472**, 69 (2011).

[67] P. E. Barclay, K. Srinivasan, and O. Painter, Opt. Express **13**, 801 (2005).

[68] W. H. P. Pernice, C. Schuck, M. Li, and H. X. Tang, Opt. Express **19**, 3290 (2011).

[69] I. Shomroni, A. Youssefi, N. Sauerwein, L. Qiu, P. Seidler, D. Malz, A. Nunnenkamp, and T. J. Kippenberg, Phys. Rev. X **9**, 041022 (2019).
[70] C. U. Lei, A. J. Weinstein, J. Suh, E. E. Wollman, A. Kronwald, F. Marquardt, A. A. Clerk, and K. C. Schwab, Phys. Rev. Lett. **117**, 100801 (2016).
[71] G. A. Peterson, F. Lecocq, K. Cicak, R. W. Simmonds, J. Aumentado, and J. D. Teufel, Phys. Rev. X **7**, 031001 (2017).
[72] N. R. Bernier, L. D. Tóth, A. Koottandavida, M. A. Ioannou, D. Malz, A. Nunnenkamp, A. K. Feofanov, and T. J. Kippenberg, Nat. Commun. **8**, 604 (2017).
[73] T. A. Palomaki, J. W. Harlow, J. D. Teufel, R. W. Simmonds, and K. W. Lehnert, Nature (London) **495**, 210 (2013).
[74] T. A. Palomaki, J. D. Teufel, R. W. Simmonds, and K. W. Lehnert, Science **342**, 710 (2013).
[75] https://doi.org/10.5281/zenodo.3741836.